Article

Recognition of Stator Winding Inter-Turn Fault in Interior-Mount LSPMSM Using Acoustic Signals

Luqman S. Maraaba [1,*] **, Ssennoga Twaha** [2,3]**, Azhar Memon** [1] **and Zakariya Al-Hamouz** [4]

1   Center for Engineering Research, Research Institute, King Fahd University of Petroleum and Minerals, Dhahran 31261, Saudi Arabia; azhar.memon@kfupm.edu.sa
2   Department of Electrical and Electronic Engineering, Faculty of Engineering, Kyambogo University, Kyambogo P.O. Box 01, Uganda; twaha.ssennoga1@nottingham.ac.uk
3   Department of Architecture and Built Environment, Faculty of Engineering, University of Nottingham, Nottingham NG7 2RD, UK
4   Department of Electrical Engineering, Faculty of Engineering, Indiana Institute of Technology, Washington Blvd., Fort Wayne, IN 46803, USA; zmal-Hamouz@indianatech.edu
*   Correspondence: lmaraaba@kfupm.edu.sa; Tel.: +966-138-602-545

check for updates

Abstract: This paper presents a novel stator inter-turn fault diagnosis method for Line Start Permanent Magnet Synchronous Motors (LSPMSMs) using the frequency analysis of acoustic signals resulting from asymmetrical faults. In this method, acoustic data are experimentally collected from a 1 hp interior mount LSPMSM for different inter-turn fault cases and motor loading levels, while including the background noise. The signals are collected using a smartphone at a sampling rate of 48,000 samples per second. The signal for each case is analyzed using fast Fourier transform (FFT), which results in the decomposition of the signal into its frequency components. The results indicate that, for both no-load and full-load conditions, 39 components are observed to be affected by the faults, whereby their amplitudes increase with the fault severity. The 40-turns fault shows the highest difference in the component amplitudes compared with the healthy condition acoustic signal. Therefore, this diagnostic method is able to detect the stator inter-turn fault for interior mount LSPMSMs. Moreover, the method is simple and cheap since it uses a readily available sensor.

Keywords: electric motor; inter-turn fault; acoustic signals

1. Introduction

Electric motors play a crucial role in industry as they are used to run different industrial processes during the manufacturing of different products. Therefore, the types of motors have greatly increased in recent years, with induction motors being the most widely used in industry today [1]. In some industrial applications, particularly in oil and gas, induction motors are gradually being substituted by line-start permanent magnet synchronous motors (LSPMSMs) [2]. The LSPMSM has several advantages over other motors, including being high-efficiency, having a power factor within a wide load range, and being equipped with a squirrel cage that rotates the rotor from standstill, with magnets that help the motor to maintain a synchronous speed.

Because of external and internal stresses, for example, voltage stresses, insulation material destruction, inefficient cooling, chemical contamination, partial discharge, and overloading, motors are exposed to a variety of faults. Inter-turn faults, broken bars, eccentricity, and demagnetization are some of the main failures. Based on Electric Power Research Institute (EPRI) and IEEE studies, insulation breakdown is the main cause of inter-turn faults [3,4]. Normal manufacturing processes and operation are affected by such failures, as these result in the loss of revenue due to a reduced volume and

quality of products from the production lines. Moreover, the reliability and efficiency of the motors are negatively affected by some of these faults.

While carrying out the diagnosis of machines, several techniques are employed to process data. Some techniques are based on feature extraction whereas others deal with the classification of the processed data. Additionally, various forms of signals are also used for fault diagnosis [5], including magnetic, acoustic [6], electric [7], and thermal signals [8]. The objective of model-based methods is to generate effects identical to the ones observed in daily life by using similar loading at the fault location [9]. These models are mainly based on the information obtained from process models, signal models, or even directly measured signals. Vibration methods such as the simple Jeffcott rotor model and Finite Elements Method (FEM) are also available, with which the faults are detected by analyzing the variations in the response [10]. The signals examined through these approaches may be generated through models or from real systems. However, the traditional FEM is associated with a lot of issues, such as slow convergence, limited accuracy, nonlinearity, and lower efficiency. Although vibration measurement is considered to be the most popular method in the condition monitoring of rotating machines, acoustic emission signals are noted to be superior in low speed rotation systems and the early detection of faults [11].

Furthermore, a variety of faults occurring in different types of machines are discussed. Several research studies have been carried out regarding the diversity of analytical techniques, parameters used for fault detection, and types of faults. For static eccentricity faults in a PMSM, [12] a spectral analysis technique is used for the current as well as the voltage, torque, and speed parameters to detect the faults. In another study, for a similar fault in a three-phase LSPMSM, [13] investigated the use of the power spectral density of the stator current to detect the fault. In [14], a finite element model for an LSPMSM under static eccentricity was used to investigate the static eccentricity fault by applying the time domain analysis of the stator current. A set of statistical features—such as the mean, skewness, kurtosis, and standard deviation—that are highly affected by the fault were calculated using the current signal. The study recommended the consideration of these distinct changes in fault detection. In [15], the static, dynamic, and mixed eccentricity faults in an LSPMSM were investigated using the finite element model under no-load and full-load conditions. The instantaneous speed was used to investigate the effects of the faults on the transient behavior of the motor. In [16–18], a neural-network-based diagnostic tool for detecting inter-turn faults in an LSPMSM was developed that uses three cycles of the steady-state stator current for detecting the fault. The authors in [16,18] detected the severity of fault, while in [17], the phase location and severity of the fault were detected by using the three-phase currents. It worth mentioning that, in [17], a JMAG™-based finite element mathematical model was developed and utilized to analyze the fault as well as for the generation of training and testing data, whereas in [18], both simulation and experimental data were used. In addition, in [16,17], time and frequency domain analysis was carried out to extract the fault representative features from the current, while in [18], the three-phase instantaneous steady state current was used as an input to the convolutional neural network. It is worth mentioning that the studies performed for the detection of inter-turn faults in an LSPMSM using the stator current did not consider the case of an unbalanced supply. However, having an unbalanced power supply could affect the performance of such a detection tool, since it depends on the current, which is highly affected by the unbalanced supply [19].

To detect a broken rotor bar in an LSPMSM, [20] used time-domain analysis by applying the Hilbert transform to extract the transient current envelope. The statistical features of the transient current were used in random forests by [21], to classify the broken rotor bar fault. Alternatively, in [22] presented the analysis of the acoustic signal to detect short circuits and broken coils in a synchronous motor. The study in [22] used line spectral frequencies and the K-nearest classifier with Minkowski distance. The limitation of the proposed method is that it can only be useful for electric motors with the same parameters and size but not for different motor ratings. In [5], both the broken bars in an induction motor and shorted rotor coils in a direct motor were investigated using the acoustic signal

for different fault severities. In this study, the authors used pattern recognition on the acoustic data to detect the abnormalities. In [23], the acoustic sensors in smartphones, which are readily available for low-cost continuous real-time monitoring, were used in detecting the broken bar and dynamic eccentricity in induction motors. It was concluded that the smartphones could be used for preliminary condition monitoring for the motors. In [24], an acoustic-signal-based diagnostic tool for detecting stator winding faults in a single-phase induction motor was developed. Two types of stator winding faults were considered: an auxiliary winding short circuit fault and auxiliary-main windings short circuit fault. The authors used fast Fourier transform to extract the fault-related features, in which they analyzed the application of K-Nearest Neighbor, K-Means clustering, and Linear Perceptron classifiers. The results demonstrated the effectiveness of all the selected classifiers. In [25], a fault-detection tool for broken-bar and end-ring faults in a squirrel cage three-phase induction motor was developed. The acoustic signals collected by a digital voice recorder were used for the detection of faults. A Nearest Neighbor classifier and backpropagation neural network were implemented using a group of extracted features from the spectrum of acoustic signals for fault detection.

Due to the increase in the volume of LSPMSMs employed in industry, the need for maintenance programs is growing proportionally to promote the health of these motors. Consequently, it is important to develop diagnostic tools that can detect the faults at their early stages [26]. It is worthwhile to note that most of the previous research studies on the fault diagnosis of LSPMSMs have focused on rotor faults, eccentricity, and demagnetization [14,15,27–30], while few recent studies have been performed on stator winding faults [16–18,26].

The stator windings consist of an insulated conductor. It is reported that the stator winding faults in electric machines represent around 36% of the motor faults [1]. The main causes of stator winding faults are an inefficient cooling system, voltage stresses, overloading, short circuits between the winding, chemical contamination, and partial discharge in the winding. In most cases, the stator winding faults start as turn-to-turn faults, inter-turns faults, coil-to-coil faults, phase-to-ground faults, and phase-to-phase faults but finally result in motor failures. Therefore, it is crucial to design an effective tool for detecting such faults in the initial stage since these types of faults become worse with time if not addressed [1,26]. This fault may lead to the malfunctioning of the motor and finally take it out of operation, hence affecting the production line and the overall business operation. Therefore, this research work investigates the stator inter-turn faults in an interior-mount LSPMSM. Specifically, the acoustic signals resulting from the healthy and faulty operation of the motor are analyzed to identify the distinct features for different types of asymmetrical anomalies, as well as to characterize the loading and no-loading modes of the motor operation.

According to the literature, there is no prior work on using acoustic signals to identify the inter-turn fault in an LSPMSM. Moreover, the distinct characteristics of the sound produced by various severity levels of these faults in laboratory tests clearly indicate that there is the potential for effective asymmetrical fault diagnosis. With this motivation, the objective of this study was to carry out a study on the use of a smartphone to collect the acoustic signals resulting from inter-turn faults for full-load and no-load conditions of operation with different fault severities in an LSPMSM. The Fast Fourier transform was used to extract the highly fault-related frequency components from the collected acoustic signals.

2. Experimental Setup and Data Collection

Table 1 shows the parameters for a 1 hp interior mount LSPMSM that was used in the experiment. A smartphone was used for collecting the acoustic signals from the machine. The laboratory experimental setup for performing the tests is shown in Figure 1.

Table 1. Parameters of Line Start Permanent Magnet Synchronous Motors (LSPMSM) motor.

Parameters	Value
Number of poles	4
Number of turns per stator phase	86×4
Number of bars	20
Permanent magnet flux density	1.25 T
Machine rated power	1 hp
Rated voltage	400 Vrms
Rated frequency	60 Hz
Rated speed	1800 rpm
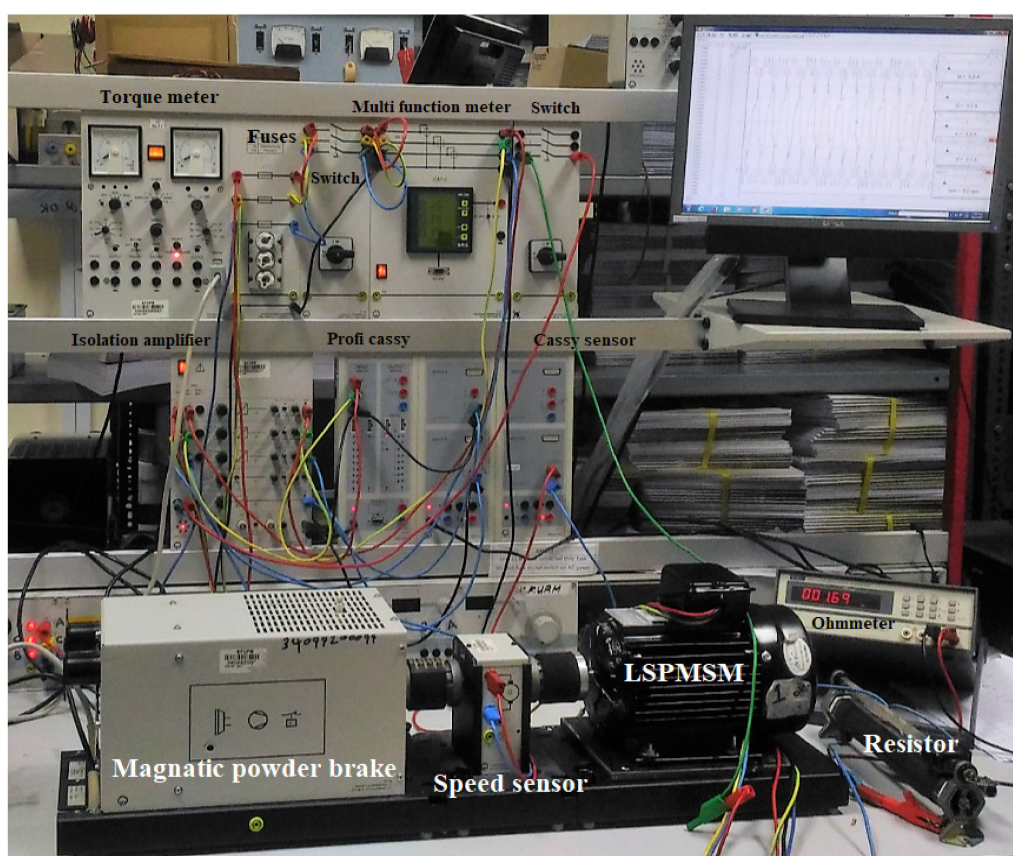
Figure 1. Laboratory LSPMSM experimental setup.

Different sizes of inter-turn faults were introduced to the tested interior mount LSPMSM. The tested cases of the motor include (i) the healthy case (no shorted turns), (ii) four shorted turns, (iii) nine shorted turns, (iv) 26 shorted turns, and (v) 40 shorted turns. It is worth mentioning that all the tested cases were performed at no load (NL) and a full load (FL) of 4 N·m with background noise, comprising the sound of other machines operating in the laboratory and human noise.

The stator inter-turn fault was achieved experimentally by adding six access points to phase-A, which are labeled with the letter k, with the subscripts representing the size of the inter-turn fault, as shown in Figure 2. For example, for the 26 shorted turns, k_1 and k_2 were connected together through a resistance (fault resistance) to limit the amount of short-circuit current in the shorted turns. A similar approach was used for the other sizes of inter-turn faults as indicated by the different colors on phase-A in Figure 2. During the experiments, all the electric data of the motor under investigation were measured and the audible noise was recorded using a smartphone mounted on the circumference of the motor at a rate 48,000 samples per second.
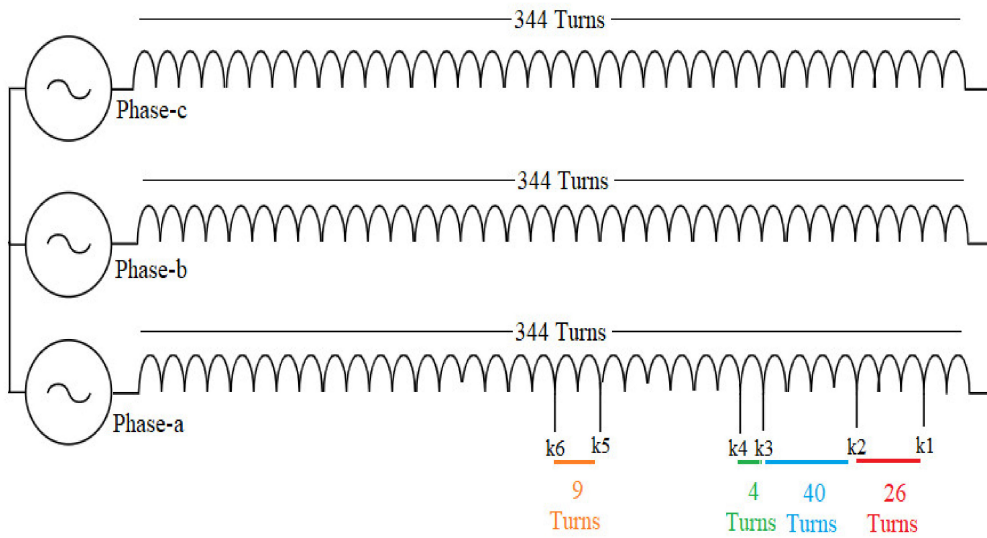
Figure 2. Fault illustration for LSPMSM experimental setup.

3. Results and Discussions

To analyze the effectiveness of the acoustic signal in detecting the occurrence of an inter-turn fault at its early stages as well as analyzing the effect of the fault on the generated sound, the acoustic signals for the different fault severities with different background noise were collected using a smartphone at 48,000 samples per second, for a duration of around 35 s each time, while the motor was operating under a no-load condition. The collected signals are indicated in Figure 3, whereas Table 2 explains the periods A through M.
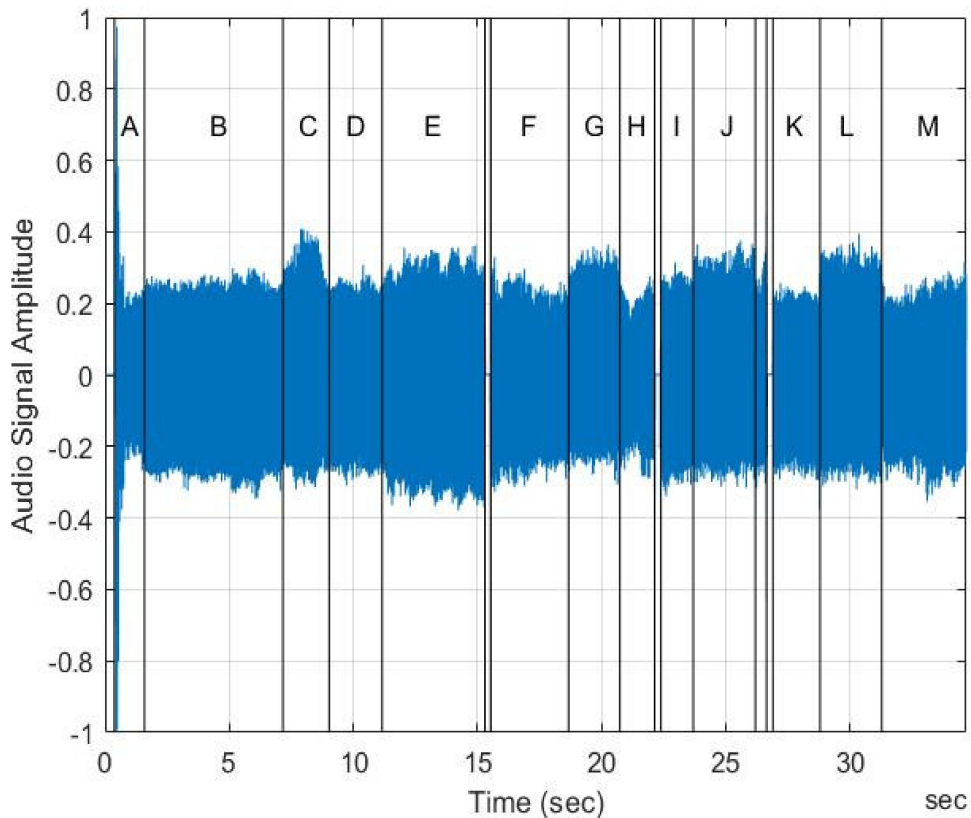
Figure 3. Motor-generated sound under different fault severities at no load.

Table 2. Description of periods in Figure 3.

Period	Description
A	Sound generated at starting in healthy condition
B, D, F, H, I, K, and M	Steady-state sound in healthy state with different background noise
C and E	9 shorted turns
G and J	26 shorted turns
L	40 shorted turns

It is clear from the figure that the generated sound is affected by the size of fault and the surrounding background noise as demonstrated by the size of the signal in a given period. For example, the signal period L for the 40 shorted turns fault is higher than that for the signal period K for the steady-state sound with background noise in the healthy state.

To differentiate between the effects of the fault, background noise, and sound for the healthy condition, the spectrogram of the captured signal is shown in Figure 4, with the magnitude of the frequency content with respect to time during the recorded period. It is clear that most of the energy is concentrated under 15 kHz in frequency, regardless of the fault size and operating conditions. This is indicated by the yellow-colored region of the spectrum, which is mainly above a power spectral density of −80 dB/Hz. This means that the signals or vibrations are stronger in this region of the spectrum. Therefore, this study focused on this area to find the fault-related features.
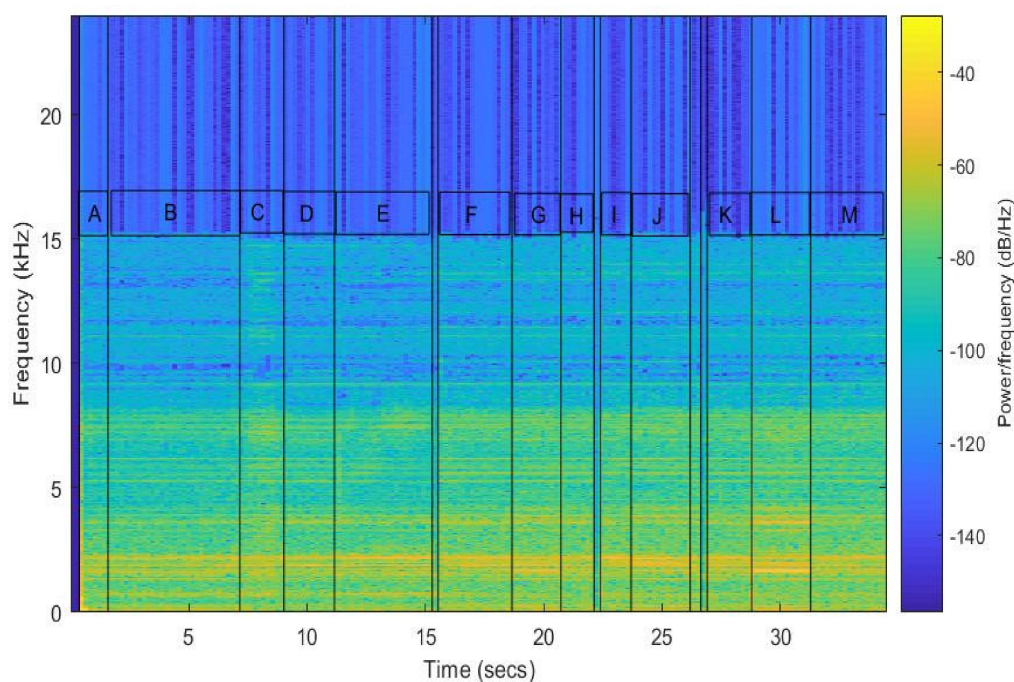
Figure 4. Spectrogram of motor-generated sound under different fault severities at no load.

In order to extract the distinct frequency components related to the inter-turn faults and their severity under loading and non-loading conditions, ten operating cases were considered: five shorted-turn cases for a full-load condition and another five for a no-load condition, whereby each of them was collected for a period of two seconds, representing 96,000 samples at a sampling frequency of 48,000 samples per second. The considered cases include (i) the healthy case (no shorted turns), (ii) 4 shorted turns, (iii) 9 shorted turns, (iv) 26 shorted turns, and (v) 40 shorted turns; these five cases were considered for a full load (FL) of 4 N·m and repeated for the no-load (NL) conditions with background noise. It should be noted that the audible sound generated from the loaded motor differed from that of the unloaded motor.

First, the spectra of the healthy machine were analyzed and regarded as a reference. Thereafter, the spectra for the fault cases were evaluated with emphasis on the change in the amplitude of the characteristic frequencies in comparison with the reference (spectra of healthy machine). Fast Fourier transform (FFT) was applied to the originally recorded signals. Figure 5 shows the FFT for the healthy state, nine shorted turns, and 26 shorted turns under the NL condition, with the amplitudes of all the components of frequencies less than 15 kHz. It is clear that many components are affected by fault severity, where the amplitude for some is directly proportional to the severity.
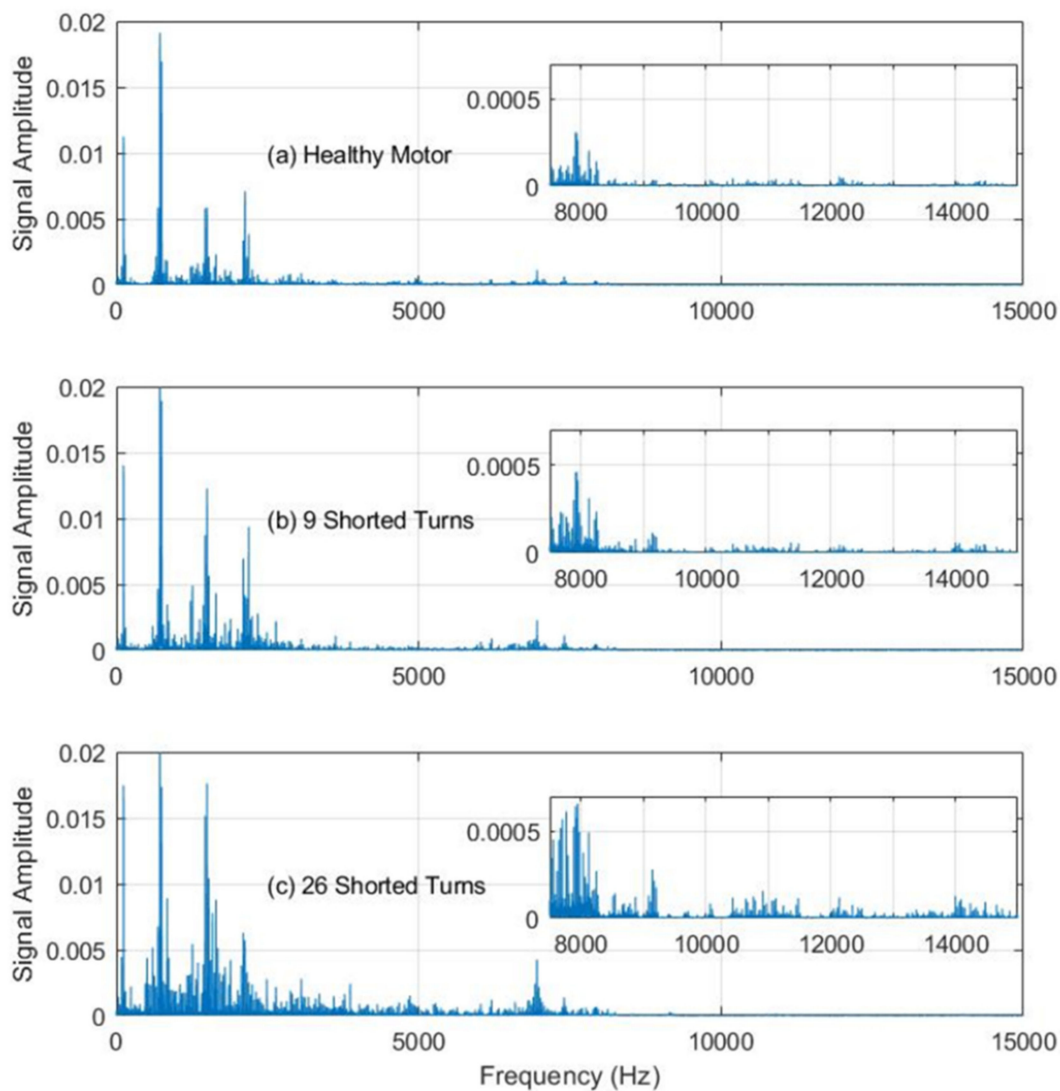
Figure 5. Fast Fourier transform (FFT) at no load: (**a**) healthy, (**b**) 9 shorted turns, and (**c**) 26 shorted turns.

The spectra inside the subplots in Figure 5 indicate the zoomed scales of the signal between 8 and 14 kHz to indicate the invisible components affected by the fault size. A more detailed investigation of the amplitude spectra for the 10 collected cases reveals that there are some components that are highly affected by the inter-turn fault severity regardless of the motor loading condition. In total, there are 39 components that are fault-related regardless of the load and are shown in Figures 6 and 7 under no and a full load, respectively. To obtain the 39 components from the spectrum, an investigation for selecting the fault-size-related frequency components regardless of the loading levels was carried out using a deterministic approach, through nested loops in MATLAB software (2019b, MathWorks, Natick, MA, USA). It is clear from the figures that the magnitudes of these components for the healthy condition for NL and FL have slight differences. As the fault severity increases, their magnitudes

proportionally increase. This indicates that their amplitudes can be a good indicator for the detection of a fault and its severity.
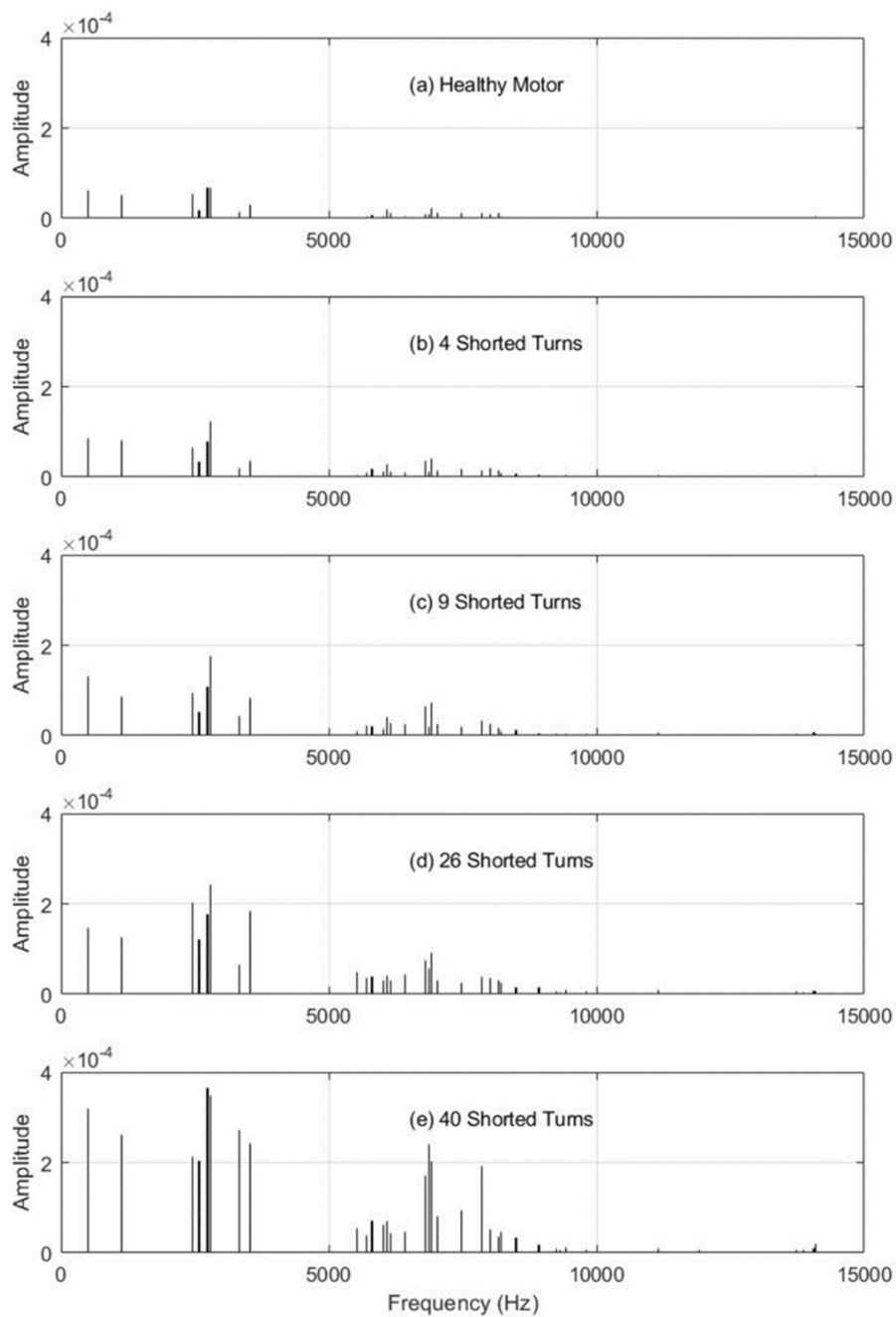

Figure 6. Distinct component amplitude at no load: (**a**) healthy, (**b**) 4 shorted turns, (**c**) 9 shorted turns, (**d**) 26 shorted turns, and (**e**) 40 shorted turns.
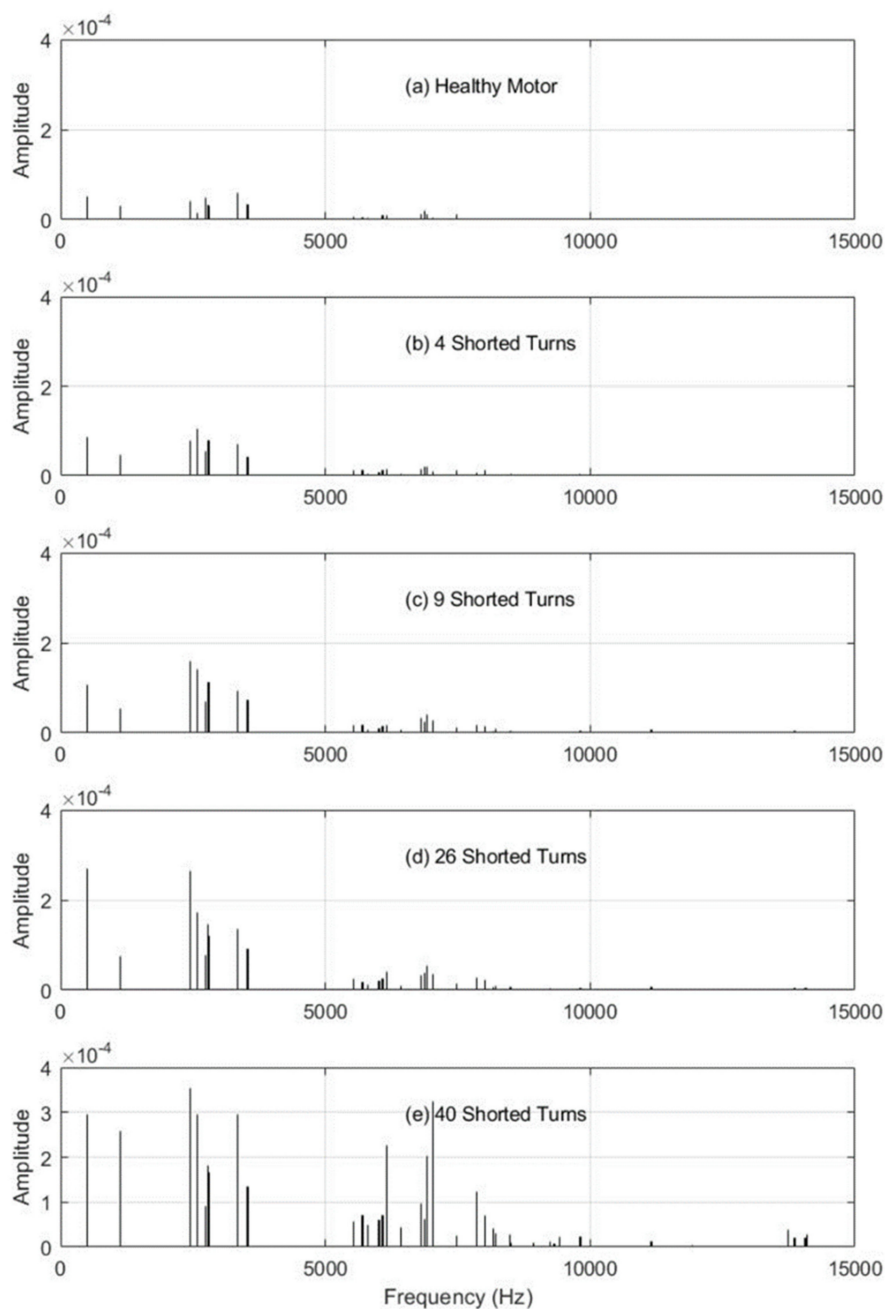
Figure 7. Distinct component amplitude at full load: (**a**) healthy, (**b**) 4 shorted turns, (**c**) 9 shorted turns, (**d**) 26 shorted turns, and (**e**) 40 shorted turns.

To analyze the selected components related to the fault, their ratios of the amplitude under the fault condition to that under the healthy condition at the same load level was calculated. Figures 8 and 9 show the amplitude ratio and frequency in kHz for each distinct frequency component for all the fault cases at no load and full load, respectively. Note that the frequencies for these components are the same in both loading conditions. In addition, both figures show that as the fault size increases, the ratio increases for most of the components, with a prominent difference noted for the 40-shorted-turns fault. The amplitude is thus the indicative parameter for the fault severity. As seen in Figure 8, the most affected frequency components at no load are 5.53, 6.80, 8.50, 8.93, 9.82, 11.16, 11.92 and 14.06 kHz, while Figure 9 shows those at full load, which include 2.58, 6.02, 7.03, 7.85, 8.01, 8.5, 13.73 and 14.09 kHz. For the no-load condition, the most affected components are nearly above 9 kHz, while those for the full-load condition are roughly below 9 kHz. Therefore, to diagnose a motor at no load, the emphasis

is put on the frequency components below 9 kHz, whereas for a full load, the engineers should look at those between about 6 and 9 kHz. This indicates that having a load will dampen the high frequency sound generated from the motor and, hence, affect the fault at frequencies lower than 9 kHz.
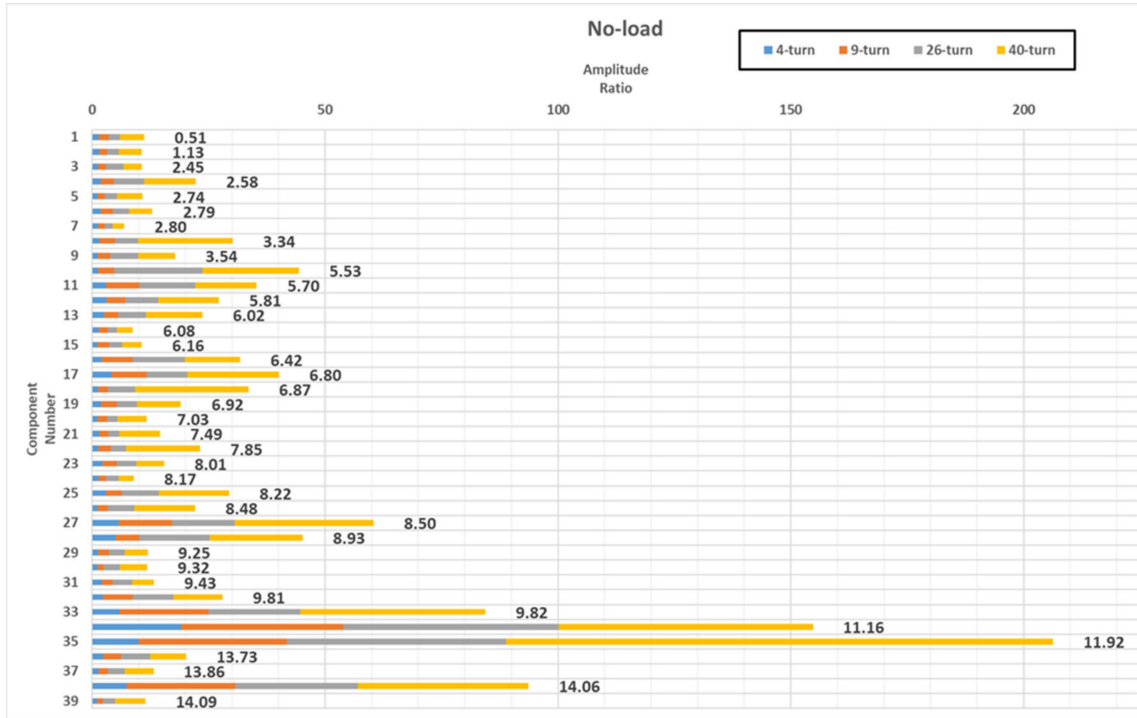

Figure 8. Frequency components' amplitude ratios at no load. Labels show the frequencies in kHz.
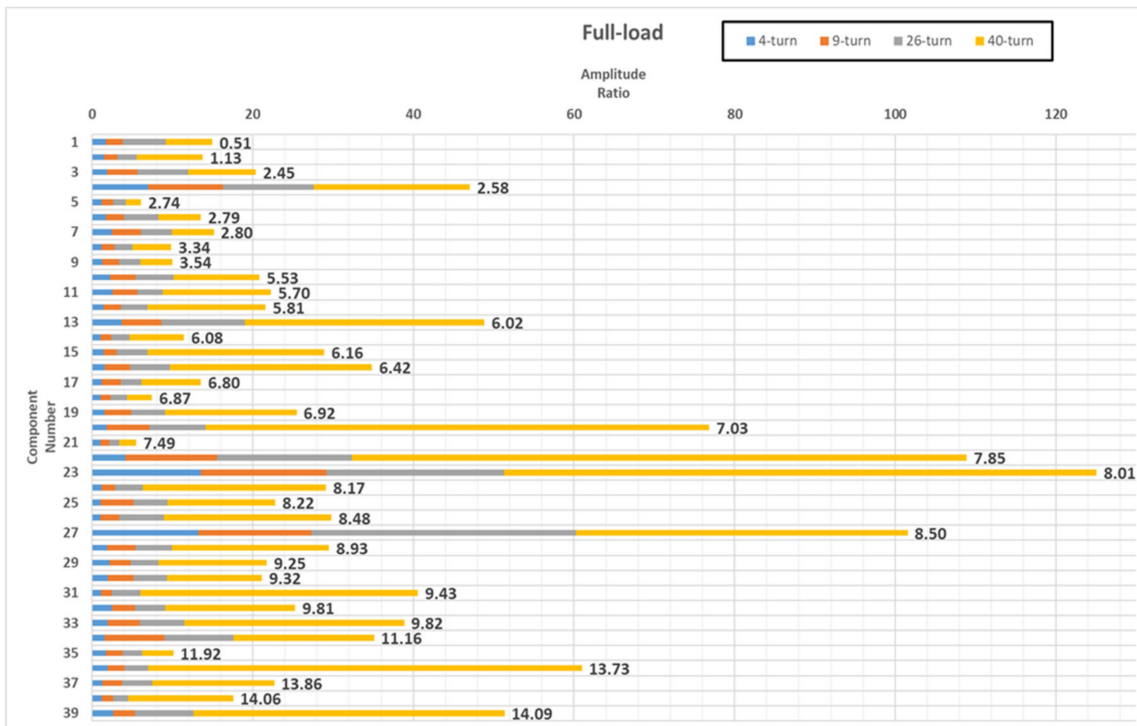

Figure 9. Frequency components' amplitude ratios at full load. Labels show the frequencies in kHz.

4. Conclusions

This paper presents a novel stator inter-turn fault diagnosis method for LSPMSMs using the frequency analysis of the acoustic signals resulting from the faults. The experimental work was carried out in the laboratory, where the acoustic signal data were collected from a 1 hp interior mount LSPMSM for the different inter-turn fault cases and motor loading levels, while including the background noise. The tested cases of the motor include the healthy state (no shorted turns), four shorted turns, nine shorted turns, 26 shorted turns, and 40 shorted turns fault. The signals were collected using a smartphone at a sampling rate of 48,000 samples per second. The signal for each case was analyzed using FFT, which resulted in the decomposition of the signal into its frequency components. Specifically, for both the no-load and full-load conditions, 39 components were observed to be affected by the faults, whereby their amplitudes increased with the fault severity. The 40-turns fault showed the highest difference in component amplitudes compared with the healthy condition acoustic signal. Eight out of the 39 components were observed to exhibit the highest change in amplitude due to the fault severity. The components above the frequency of 9 kHz were found to be the most affected in case of no load, and those below this frequency, for a full load. Therefore, this method has been proved to clearly identify the stator inter-turn fault for LSPMSMs.

References

1. Maraaba, L.; Al-Hamouz, Z.; Abido, M. An efficient stator inter-turn fault diagnosis tool for induction motors. *Energies* **2018**, *11*, 653. [CrossRef]
2. Maraaba, L.; Al-Hamouz, Z.; Milhem, A.; Abido, M. Modelling of interior-mount LSPMSM under asymmetrical stator winding. *IET Electr. Power Appl.* **2018**, *12*, 693–700. [CrossRef]
3. Siddiqui, K.M.; Sahay, K.; Giri, V. Health monitoring and fault diagnosis in induction motor—A review. *Int. J. Adv. Res. Electr. Electron. Instrum. Eng.* **2014**, *3*, 6549–6565.
4. Kong, T.; Kim, H.; Park, H.; Lee, S.; Park, J. Changes in insulation characteristics of high-voltage motor stator windings with temperature and moisture. *Am. J. Electr. Power Energy Syst.* **2018**, *7*, 62–67. [CrossRef]
5. Glowacz, A. Diagnostics of DC and induction motors based on the analysis of acoustic signals. *Meas. Sci. Rev.* **2014**, *14*, 257–262. [CrossRef]
6. Glowacz, A. Acoustic-based fault diagnosis of commutator motor. *Electronics* **2018**, *7*, 299. [CrossRef]
7. Zappalá, D.; Sarma, N.; Djurović, S.; Crabtree, C.; Mohammad, A.; Tavner, P. Electrical & mechanical diagnostic indicators of wind turbine induction generator rotor faults. *Renew. Energy* **2019**, *131*, 14–24.
8. Al-Musawi, A.K.; Anayi, F.; Packianather, M. Three-phase induction motor fault detection based on thermal image segmentation. *Infrared Phys. Technol.* **2020**, *104*, 103140. [CrossRef]
9. Gómez, M.J.; Castejón, C.; García-Prada, J.C. Review of recent advances in the application of the wavelet transform to diagnose cracked rotors. *Algorithms* **2016**, *9*, 19. [CrossRef]
10. Wang, T.; Han, Q.; Chu, F.; Feng, Z. Vibration based condition monitoring and fault diagnosis of wind turbine planetary gearbox: A review. *Mech. Syst. Signal Process.* **2019**, *126*, 662–685. [CrossRef]
11. Caso, E.; Fernandez-del-Rincon, A.; Garcia, P.; Iglesias, M.; Viadero, F. Monitoring of misalignment in low speed geared shafts with acoustic emission sensors. *Appl. Acoust.* **2020**, *159*, 107092. [CrossRef]

12. Akar, M.; TAŞKIN, S.; ŞEKER, Ş.S.; Cankaya, I. Detection of static eccentricity for permanent magnet synchronous motors using the coherence analysis. *Turk. J. Electr. Eng. Comput. Sci.* **2010**, *18*, 963–975. [CrossRef]

13. Karami, M.; Mariun, N.; Mehrjou, M.R.; Ab Kadir, M.Z.A.; Misron, N.; Mohd Radzi, M.A. Static eccentricity fault recognition in three-phase line start permanent magnet synchronous motor using finite element method. *Math. Probl. Eng.* **2014**, *2014*. [CrossRef]

14. Dogan, Z.; KARA, B.; EMEKSIZ, C.; GOKREM, L. The static eccentricity fault diagnosis in time domain at line start permanent magnet synchronous motor. *J. New Results Sci.* **2016**, *5*, 88–95.

15. Sedky, M. Diagnosis of static, dynamic and mixed eccentricity in line start permanent magnet synchronous motor by using FEM. *Int. J. Electr. Robot. Electron. Commun. Eng.* **2014**, *8*, 29–34. [CrossRef]

16. Maraaba, L.S.; Al-Hamouz, Z.M.; Abido, M.A. An accurate tool for detecting stator inter-turn fault in LSPMSM. *IEEE Access* **2019**, *7*, 88622–88634. [CrossRef]

17. Maraaba, L.S.; Al-Hamouz, Z.M.; Milhem, A.S.; Abido, M.A. Neural network-based diagnostic tool for detecting stator inter-turn faults in line start permanent magnet synchronous motors. *IEEE Access* **2019**, *7*, 89014–89025. [CrossRef]

18. Maraaba, L.S.; Milhem, A.S.; Nemer, I.A.; Al-Duwaish, H.; Abido, M.A. Convolutional Neural Network-Based Inter-Turn Fault Diagnosis in LSPMSMs. *IEEE Access* **2020**, *8*, 81960–81970. [CrossRef]

19. Bouzid, M.B.K.; Champenois, G.; Bellaaj, N.M.; Signac, L.; Jelassi, K. An effective neural approach for the automatic location of stator interturn faults in induction motor. *IEEE Transact. Ind. Electron.* **2008**, *55*, 4277–4289. [CrossRef]

20. Mehrjou, M.R.; Mariun, N.; Karami, M.; Misron, N.; Radzi, M.A.M. Broken rotor bar detection in LS-PMSMs based on statistical features analysis of start-up current envelope. In Proceedings of the 2015 IEEE 3rd International Conference on Smart Instrumentation. Measurement and Applications (ICSIMA), Putrajaya Marriott, Malaysia, 24–25 November 2015; pp. 1–6.

21. Quiroz, J.C.; Mariun, N.; Mehrjou, M.R.; Izadi, M.; Misron, N.; Radzi, M.A.M. Fault detection of broken rotor bar in LS-PMSM using random forests. *Measurement* **2018**, *116*, 273–280. [CrossRef]

22. Glowacz, A. Diagnostics of synchronous motor based on analysis of acoustic signals with the use of line spectral frequencies and K-nearest neighbor classifier. *Arch. Acoust.* **2014**, *39*, 189–194. [CrossRef]

23. Vaimann, T.; Sobra, J.; Belahcen, A.; Rassõlkin, A.; Rolak, M.; Kallaste, A. Induction machine fault detection using smartphone recorded audible noise. *IET Sci. Meas. Technol.* **2018**, *12*, 554–560. [CrossRef]

24. Glowacz, A. Acoustic based fault diagnosis of three-phase induction motor. *Appl. Acoust.* **2018**, *137*, 82–89. [CrossRef]

25. Glowacz, A.; Glowacz, Z. Diagnosis of stator faults of the single-phase induction motor using acoustic signals. *Appl. Acoust.* **2017**, *117*, 20–27. [CrossRef]

26. Maraaba, L.S.; Al-Hamouz, Z.M.; Abido, M.A. Mathematical modeling, simulation and experimental testing of interior-mount LSPMSM under stator inter-turn fault. *IEEE Transact. Energy Convers.* **2018**, *34*, 1213–1222. [CrossRef]

27. Shen, J.-X.; Li, P.; Jin, M.-J.; Yang, G. Investigation and countermeasures for demagnetization in line start permanent magnet synchronous motors. *IEEE Transact. Magn.* **2013**, *49*, 4068–4071. [CrossRef]

28. Lei, C.; Changjiang, W.; Xiaohua, B. Influence of load characteristics on the demagnetization of LSPMSM with non-uniform air gap structure. *J. Electr. Eng.* **2018**, *1*, 1.

29. Weifu, L.; Haisen, Z.; Jian, Z.; Yingli, L.; Mingji, L. Dynamic irreversible demagnetization behavior of line-start permanent magnet synchronous motors in the starting process. *Electr. Power Compon. Syst.* **2015**, *43*, 1621–1629. [CrossRef]

30. Mehrjou, M.R.; Mariun, N.; Karami, M.; Noor, S.B.M.; Zolfaghari, S.; Misron, N.; Kadir, M.Z.A.A.; Radzi, M.A.M.; Marhaban, M.H. Wavelet-based analysis of MCSA for fault detection in electrical machine. In *Wavelet Transform and Some of Its Real-World Applications*; IntechOpen: London, UK, 2015; p. 79.